RESEARCH ARTICLE

Effects of Allogeneic Bone Substitute Configurations on Cell Adhesion Process *In Vitro*

Jie Liu, MD[1†], Li Yang, MD[1†], Hao Zhang, MD[1†], Jing-yu Zhang, MD, PHD[2], Yong-cheng Hu, MD, PHD[2]

[1]*Tianjin Medical University and* [2]*Tianjin Hospital, Tianjin, China*

Objective: To explore the potential effect of three allogenic bone substitute configurations on the viability, adhesion, and spreading of osteoblasts *in vitro*.

Methods: Freeze-dried cortical bone were ground and fractions were divided into three groups with different sizes and shapes, defined as bone fiber (0.1 mm × 0.1 mm × 3 mm), bone powder (0.45–0.9 mm), and bone granule group (3–6 mm). MC3T3-E1 cells were divided and co-cultured within groups to induce cell adhesion. The configuration of allogenic bone was captured by scanning electron microscopy and confocal laser scanning microscopy, and substrate roughness values were quantified. Cell adhesion rate was assessed using the hemocyte counting method, cell viability was determined by CCK-8 assay and live/dead staining, and cell morphology was visualized by Phalloidin and DAPI, and the mRNA expression of adhesion-related gene (vinculin) of different substitutes were determined with quantitative real-time polymerase chain reaction.

Results: The roughness values of bone fiber, bone powder, and bone granule group were 1.878 μm (1.578–2.415 μm), 5.066 μm (3.891–6.162 μm), and 0.860 μm (0.801–1.452 μm), respectively (bone powder group compared with bone granule group, $H = 18.015$, $P < 0.001$). Similar OD values of all groups in CCK-8 assay indicated good biocompatibility of these substitutes (bone fiber, 0.201 ± 0.004; bone powder, 0.206 ± 0.008; bone granule group, 0.197 ± 0.006; and the control group, 0.202 ± 0.016, $F = 0.7152$, $P > 0.05$). In addition, representative cell adhesion rates at 24 h showed significantly lower cell adhesion rate in bone fiber group ($20.3 \pm 1.6\%$) compared to bone powder ($29.3 \pm 4.4\%$) and bone granule group ($27.3 \pm 3.2\%$) ($F = 10.51$, $P = 0.009$ and $P = 0.034$, respectively), but there was no significant difference between the latter two groups ($P > 0.05$). Interestingly, the expression of vinculin mRNA steadily decreased in a time-dependent manner. The vinculin expression reached its peak at 6 h in each group, and the vinculin levels in bone fiber, bone powder, and bone granule group were 2.119 ± 0.052, 3.842 ± 0.108, and 3.585 ± 0.068 times higher than those in the control group, respectively ($F = 733.643$, all $P < 0.001$). Meanwhile, there was a significant difference in the expression of target gene between bone powder and bone granule group ($P = 0.006$).

Conclusion: All allogenic bone substitutes presented an excellent cell viability. Moreover, bone powder and bone granule group were more likely to promote cell adhesion and spreading compared to bone fiber group.

Key words: adhesion; allogenic bone; configuration; F-actin; roughness; vinculin

Introduction

Allogenic bone has been extensively applied as an alternative to autologous bone due to its abundant source and easy availability, accounting for nearly one-third of all bone graft materials used in America[1]. Its porous structure is suitable for bone growth, and its matrix proteins, such as collagen, provide the osteo-conductive substitutes[2,3]. Despite its immune rejection and disease transmission, freeze-dried

Address for correspondence Jing-Yu Zhang, Department of Bone and Soft Tissue Oncology, Tianjin Hospital; No. 406, Jiefang Southern Road, Hexi District, Tianjin 300211, China. Email: 18631595030@163.com Yong-Cheng Hu, Department of Bone and Soft Tissue Oncology, Tianjin Hospital; No. 406, Jiefang Southern Road, Hexi District, Tianjin 300211, China. Email: huycdoctor@163.com
[†]Jing-yu Zhang and Yong-cheng Hu authors contributed equally.
Received 28 February 2021; accepted 17 June 2022

allogeneic bone substitutes possess osteo-conductive, osteo-inductive, and osteogenic properties required for successful bone repair. Extensive studies have therefore been conducted on various modifications of allogenic bone to develop bone materials with high osteogenic capacity, which is of major clinical and social importance. Lin *et al.* developed a new bone repair material generated by cross-linking heparin with allogenic bone, which not only improves its BMP-2 binding capacity, inducing differentiation of cells on the scaffold and favoring the osteogenic phenotype *in vivo*, but dramatically increases the mechanical strength that hinders the wide application of allogenic bone[4]. Shi *et al.* in 2006 constructed a functionalized bone substitute by combining the application of the demineralized bone matrix (DBM) and collagen-binding stromal-cell-derived factor-1α (CBD-SDF-1α) that is biocompatible and biodegradable[5]. CBD-SDF-1α-modified DBM scaffolds could promote bone regeneration by recruiting endogenous stem cells based on the data from immunofluorescence analysis and micro-CT.

Nevertheless, bone regeneration around newly implanted biomaterial is a complex process, which in its early phases involves the interactions between osteoblasts and the material in the host implant site, which would subsequently influence the adhesion, proliferation, and differentiation of cells. It is well-known that the initial adhesion is the first step of cell-substitute interaction in triggering the downstream behavior of cells, such as proliferation and differentiation *in vitro*, which in turn affects osseointegration *in vivo*[6]. In addition, adhesion, a sophisticated physiological process, involves a series of physiochemical changes ranging from molecule level and cellular level[7]. Lynch *et al.* suggested that integrin family receptors on the cell membrane surface specifically recognize the order of amino acids, growth factors, and adhesion-related factors in the extracellular matrix. Meanwhile, the interaction of cells with proteins adsorbed on the surface of the material mediates cell adhesion[8].

These findings indicated the properties of bone graft materials, such as roughness, pore size and porosity, hydrophilicity/hydrophobicity, surface charge, geometry, and surface bioactive molecules (proteins, peptides), played a major role in cell adhesion and subsequent biological behavior. Favorable adhesion would facilitate cell proliferation and differentiation and improve early osseointegration between bone tissue and implanted biomaterials[9]. Lin *et al.* have shown that titanium with rougher surfaces is more conducive to promoting primary cell adhesion compared with smooth surfaces, resulting in the promotion of osteoblast differentiation and bone formation[10]. Dozza *et al.* designed a series of *in vitro* and *in vivo* studies to evaluate whether particle size (large, 1–2 mm; middle, 0.5–1 mm; small, <1 mm) affects the collagen structure, cytocompatibility, and osteoinductivity of allogenic bone[11]. Although all DBM particles revealed an optimal cytocompatibility, middle size group displayed a preferable trend in almost all biological characteristics tested. Moreover, failure of osteoblasts adhesion would pose the low proliferation and cell anoikis, impeding the subsequent bone formation, and leading to a failed early osseointegration[12]. Despite the promising clinical results achieved with bone grafts, few studies focused on osteoblast adhesion *via* estimating the configuration change of allogenic bone substitutes[13].

Consequently, there is a critical need to determine the effect of different allogenic bone substitute configurations on cell adhesion process of osteoblasts and its molecule mechanism. Preparation of allogenic bone substitutes of distinct sizes and morphologies from human long bones are needed for the following purposes: (i) determining the configuration of allogenic bone (bone fiber, bone powder, and bone granule group); (ii) investigating the behavior of osteoblasts to these different configurations of allogenic bone *in vitro*; and (iii) exploring the surface morphological characteristics of allogenic bone that are most favorable for cell adhesion.

Materials and Methods

Preparation Technique and Characterization of Allogenic Bone Substitutes

Freeze-dried cortical bones of the similar adult cadavers were obtained from Beijing Wonderful Medical Biomaterials Co. (Beijing, China), each of which was prepared in strict accordance with institutional guidelines. Briefly, the soft tissue and marrow of the long cortical bones were thoroughly cleaned and removed, and their midshafts were cut into uniformly sized sections (about 10–50 cm in length), which were then treated with a high-speed rotary cutting mill (Model RRH-A1000, Shanghai Yuanwo Industrial & Trading Co., Ltd., China) and sterilized scissors (straight tip 180 mm) to obtain the following three different fractions: (i) bone fiber group (0.1 mm × 0.1 mm × 3 mm) (Figure 1A); (ii) bone powder group (0.45–0.9 mm) (Figure 1B); and (iii) bone granule group (3–6 mm) (Figure 1C); and (iv) a negative control group containing cells in absence of bone substitutes. Packaged samples (2.00 ± 0.01 g per package) were finally re-sterilized by irradiation with 25 KGy of γ radiation.

To characterize the topography of undecalcified bone scaffolds, images were recorded using high resolution scanning electron microscopy (SEM, S4800, Zeiss, Berlin, Germany) microscope at a voltage of 2 kV. Bone substitutes were fixed with 2.5% glutaraldehyde solution (Beyotime, Haimen, China) for 12 h and then dehydrated with gradient ethanol (ethanol: water, v/v, 50%, 75% and 95%, respectively) for 15 min. The as-prepared substitutes were examined by SEM after vacuum drying and gold spraying. Besides, the surface roughness parameter, the average roughness (Sa, μm), was measured and recorded by scanning an area of 690 x 520 μm^2 using a confocal laser scanning microscopy (CLSM, Leica, Germany).

Cell Culture, Seeding, and Morphological Observation

Mouse pre-osteoblastic MC3T3-E1 cells were harvested from the Tianjin Institute of Integrated Traditional Chinese and Western Medicine. Briefly, the cryopreservation cells referred

Fig. 1 Clinical macro pictures of the configuration of allogenic bone substitutes including bone fibe (A), bone powder (B), and bone granule group (C). The ruler shows a length reference in centimeters

to as "passage 1" (P1) were rapidly thawed in 37°C water bath for 3 min, followed by 1000 rpm centrifugation for 5 min, re-suspension and cultured in Dulbecco's Modified Eagle Medium (DMEM, Gibco, Thermo Scientific, Waltham, Massachusetts, USA, Lot. No. 8120350) supplemented with 10% fetal bovine serum (FBS, Gibco, Thermo Scientific, Waltham, Massachusetts, USA), and 1% (v/v) penicillin/streptomycin. Cells were incubated at 37°C in a humidified 5% CO_2 incubator and the medium was changed every 2 days. Moreover, the primary cells were routinely trypsinized with 0.25% (w/v) trypsin (Beyotime, No. C0205, Haimen, China) and passaged 1:3 upon reaching 80% confluence on the culture flask.

The cells of passage 4–6 (P4-P6) were harvested and prepared for subsequent experiments. Similar to that reported by Dozza *et al.*[11], cells were seeded on allogenic bone substitutes *via* a two-step seeding procedure. Briefly, each bone substitute was placed in 96-well plates (Corning, USA) used as a seeding vessel, and a small volume of DMEM was added to each well to ensure complete submersion of the bone. Bone substitutes were transferred to 6-well and 24-well plates (Corning, USA) after 24 h, mixed by adding different concentrations of concentrated cell suspensions (1×10,^{3} 1×10^4 and 1×10^5 cells/well, respectively) as well as repeated blowing and aspiration. They were finally placed in a humidified incubator. After being co-cultured with various bone substitutes for 6, 12, 24, and 48 h, cells were rinsed thoroughly with phosphate-buffered saline (PBS, No. C0221A, Beyotime, Haimen, China) and then observed under an Olympus phase contrast microscope equipped with a digital camera (Olympus, Tokyo, Japan).

Cell Viability

Cell viability was used for assessing the biocompatibility of these substitutes with Live and Dead Viability/Cytotoxicity Assay Kit for Animal Cells (US Everbright Inc., Lot. No. S-2014, Suzhou, China) and Cell Counting Kit (CCK-8, Yeasen Biotech, Cat. No. 40203ES76, Shanghai, China). For live/dead staining, the Calcein Acetoxymethyl Ester (Calcein-AM) presenting green-fluorescent was utilized to detect esterase activity within live cells while the Ethidium homodimer-1 (EthD-1) presenting red-fluorescent was applied for staining dead cells. At various time intervals (6, 12, 24, and 48 h) the substrates seeded with cells were rinsed and stained with 2 μM Calcein AM and 4 μM EthD-1 at room temperature for 15 min before being visualized under an inverted fluorescence microscope (Leica DMI4000 B, Wetzlar, Germany).

Cell viability was also determined by CCK-8 assay, a generally accepted colorimetric assay, according to the manufacturer's instruction, which is in addition to fluorescence observation. Briefly, the cells were seeded into 96-well plates (1×10^3 cells/well) and cultured with bone substitutes at 37°C for 24 h. Bone substitutes were transferred into new wells to avoid the influence of unattached cells prior to measurement. After being incubated with CCK-8 solutions (10 μL) for another 4 h, cells were imaged and the absorbance values were measured *via* a SpectraMax M5 microplate reader (Molecular Devices, Sunnyvale, CA, USA) at the wavelength of 450 nm. Five replicates samples were collected for each group at the different time points.

Cell Adhesion Rate Assay

After three allogenic bone substitutes were transferred to six-well plates, cells were seeded with a concentration of 1×10^6 cells/mL and co-cultured for 24 h. Allogenic bone substitutes were then removed, cells were trypsinized with 0.25% (w/v) Trypsin in six-well plates (Corning, USA), centrifuged and resuspended in a new six-well plate to a final volume of 5 mL. Using the hemocyte counting method, an aliquot of 50 μL cell suspension was finally calculated to compare the adhesion rate of the cells seeded onto different substitutes.

F-Actin Immunofluorescence

For observation of cell adhesion process, cells were seeded in 24-well plates (1×10^4 cells/well) and co-cultured with allogenic bone in DMEM for 6, 12, 24, and 48 h. The tested samples were rinsed and fixed with 4% (w/v) paraformaldehyde (Biosharp, No. BL539A, Hefei, China) at room temperature, and the cell membrane was permeabilized with 0.5% (v/v) Triton x-100 (Solar Bio, Beijing, China) at 4°C for 10 min.

The adherent cells were finally labeled for F-actin and nuclei using YF Dye Phalloidin Conjugates (US Everbright Inc., Lot. No. YP0060-300T, Suzhou, China) and DAPI (Beyotime, No. C1002, Haimen, China) in the dark at room temperature for 20 min and 5 min, respectively. Cells were

finally visualized by an inverted fluorescence microscope (Leica DMI4000 B, Wetzlar, Germany).

RNA Extraction and Quantitative Real-Time Polymerase Chain Reaction (qPCR) Analysis

Total RNA was extracted from four groups using TRIzol reagent (Beyotime, Haimen, China) according to the manufacturer's instructions. The first-strand complementary DNA (cDNA) was generated from 2 μg RNA using GoScript™ Reverse Transcription Mix (Promega Corporation, Lot. No. 0000422217, Madison, WI, USA), and qPCR were performed on a Roche Light Cycler 480 Instrument II using AceQ® qPCR SYBR Green Matrix Mix (Vazyme, Cat. No. Q111-02/03) to detect DNA levels. Each PCR reaction (20 μL) contained the following: 2x AceQ qPCR SYBR Green Matrix Mix (10.0 μL), target forward primer (0.4 μl), target reverse primer (0.4 μL), cDNA synthesis reaction (4 μL, 60 ng cDNA), and nuclease-free PCR-grade water (5.2 μL) to adjust final volume. PCR cycle conditions were as follows: 94°C for 10 min, 95°C for 10 s, 60°C for 10 s, 95°C for 15 s, 60°C for 60 s, 95°C for continue. And 40 cycles were used for PCR and quantification of target genes. The following amplification primers was used: (i) Vinculin, forward 5'-GGC TGT GGC TGG AAA CAT CTC TG-3′, reverse 5'-CTG GTG GAG GAG GCG GGA AG-3′ (Sangon Biotech, Shanghai, China, Cat. NO. 1924524060,1,924,524,061); (ii) Mouse glyceraldehyde-3-phosphate dehydrogenase (GAPDH) Endogenous Reference Genes Primers applied a commercial product (Sangon Biotech, Cat. No. B661301 - B661310, Shanghai, China).

Data from each sample were identified by melting curve analysis and normalized to GAPDH. The vinculin expression levels of the cells were normalized by GAPDH and defined as the fold change relative to the control group in the absence of the substitutes.

Observation Indicators

Surface Roughness of the Materials

The Sa value is the most commonly used parameter for surface roughness, which corresponds to the arithmetic average of the absolute values of the surface height deviations measured from the best fitting plane, according to the "Geometrical product specifications (GPS)—Surface texture: Areal—Part 2: Terms, definitions and surface texture parameters" (ISO 25178-2:2012).

The roughness values (Sa) of the material were inversely proportional to the surface smoothness of the material, and recorded using CLSM.

Cell Viability

Live/Dead Staining

Cell viability, the percentage of healthy cells in the sample population, was assessed using two fluorescent dyes, i.e., Calcein AM and EthD-1. Actually, this fluorescent kit is a two-color fluorescence cell viability assay based on the simultaneous determination of live and dead cells with two probes that measure recognized parameters of cell viability: intracellular esterase activity and plasma membrane integrity.

Bone substitutes with cells were finally visualized under an inverted fluorescence microscope. In the fluorescent pictures, the more green-stained live cells and the less red-stained dead cells reflected the stronger cell activity and lower cytotoxicity on the material.

Optical Density (OD) Values from CCK-8 Assay

Cell viability was also determined by CCK-8 assay, which provides by far the easiest and most sensitive means for performing a quantitative cell viability assay or cytotoxicity assay in mammalian cells.

After being cultured for 24 h, cells were imaged and OD values were then measured *via* a SpectraMax M5 microplate reader at the wavelength of 450 nm.

OD values are directly proportional to the number of living cells, with higher OD values indicating a larger number of living cells on the materials and better biocompatibility.

Cell Adhesion Rate

Cell adhesion rate was calculated as the number of cells adhering to the material, divided by the total number of cells used for seeding. This rate in four different fields was counted using an indirect method and calculated as follows:

$$P = 100\% \times \left(1 - \frac{M2 \times N2}{M1 \times N1}\right)$$

where *M1* and *M2* represent the volume of cell suspension added (1 mL) and mixture including washing solution and digestion solution (5 mL), respectively, while *N1* and *N2* represent the concentration of cell suspension (1×10^6 cells/mL) and unattached cells, respectively.

The magnitude of rate value was positively correlated with the ability of the bone material to adsorb osteoblasts, that is, the higher adhesion rate, the stronger adhesion ability of the material.

Cytoskeleton Morphology

The actin microfilament (F-actin) is a structural and functional component of the cell cytoskeleton that refers to the protein fiber network framework in eukaryotic cells.

F-actin was visualized with fluorescence microscopy application and microfilaments rhodamine-conjugated phalloidin staining.

A material with good affinity allows the cells to adhere to the material as quickly as possible and to extend the cytoskeleton completely, maintaining normal cell morphology and full function.

Adhesion-Related Protein (Vinculin) Expression Levels

Vinculin, a cytoskeletal protein and adhesion plaque component protein, plays an important role in adhesion by binding and interacting with a variety of adhesion plaque proteins, cytoskeletal proteins, and participating in chemical signal transduction in cells.

PCR was used to detect the relative expression of vinculin of osteoblasts on each group of materials. Higher expression levels of vinculin show that the material tends to promote cell adhesion. Conversely, lower levels of target gene expression or even lower than the control group indicate that the material is not conducive to cell adhesion.

Statistical Analysis

Statistical analyses and plotting of graphs were performed using IBM SPSS Statistics version 26.0 for Windows (SPSS Inc.), GraphPad Prism version 8.0.2 (GraphPad Software Inc., San Diego, CA, USA), and Adobe Illustrator version 23.0 (Adobe Inc., CA, USA). Normally distributed continuous variables (OD values, and qPCR data) are presented as mean ± standard deviation (SD), non-normally distributed continuous variables (Sa values) are presented as median and interquartile range (median (IQR1-IQR3)), and categorical variables (cell adhesion rate) are converted into continuous variables and expressed as percentage. All

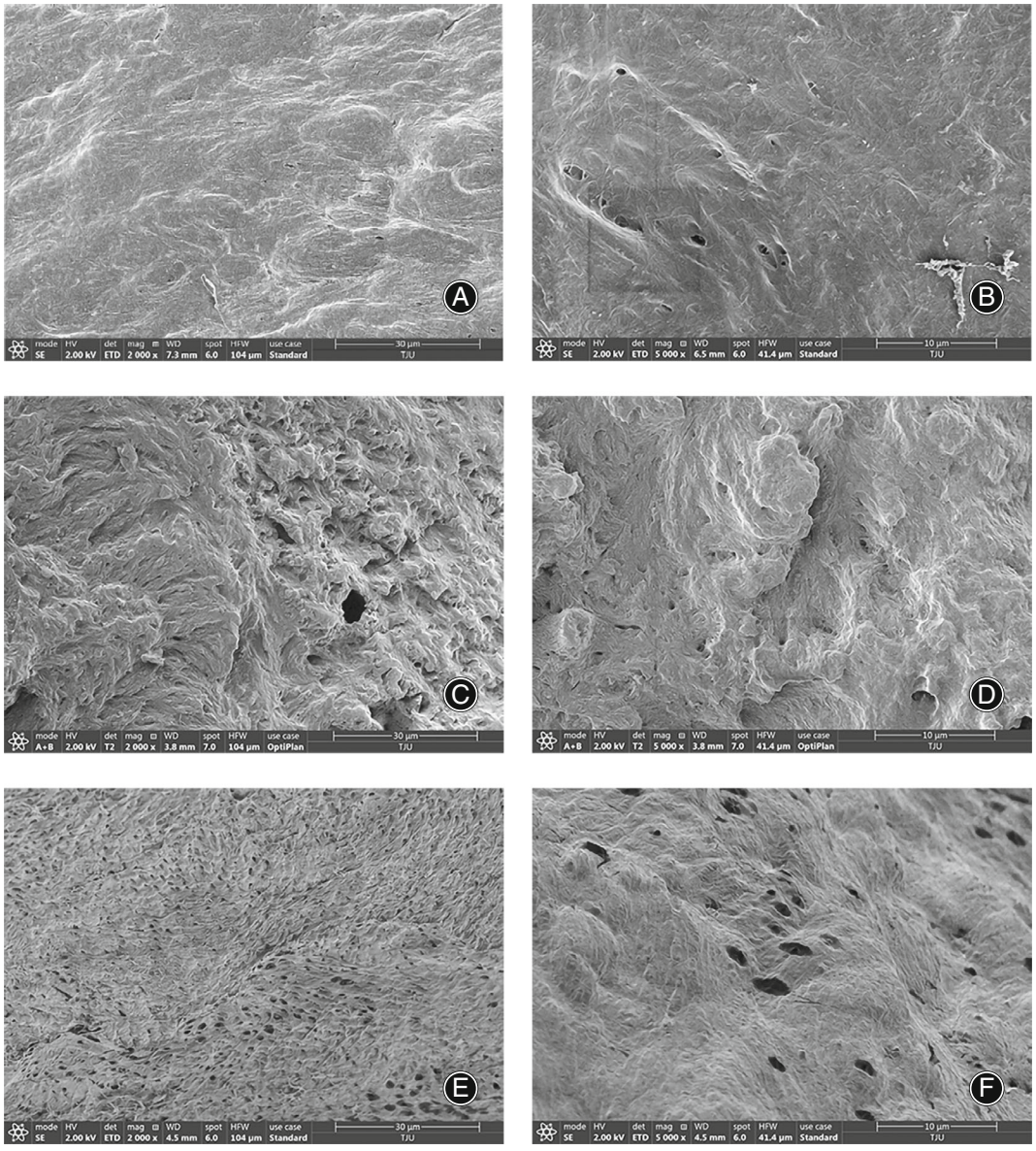

Fig. 2 Micro images of the surface topography of allogenic bone substitutes, including bone fiber (A and B), bone powder (C and D), bone granule group (E and F) *via* SEM at 2000 x (left panels) and 5000 x (right panels), respectively. Scale bar: 30 μm (A, C and E) and 10 μm (B, D and F)

data were analyzed by one-way analysis of variance (ANOVA), followed by LSD-t test for variance homogeneity and Kruskal-Wallis H test for variance heterogeneity. A two-sided *P*-value <0.05 was considered statistically significant.

Results

Material Characterization

Representative macrophotographs can be seen in Figure 1 where bone fiber (0.1 mm × 0.1 mm × 3 mm, Figure 1A) and bone powder group (0.45–0.9 mm, Figure 1B) have many small pores that are invisible to the naked eye, compared to bone granule group (3–6 mm, Figure 1C) with numerous pore structures. Furthermore, SEM and CLSM images with different morphological features are shown in Figures 2 and Figure 3. The least pore structures that appeared in bone fiber group showed the anisotropic wave-like structure on the surface of substitutes (Figure 2A, B and Figure 3A). Greater longitudinal undulating and some sharp protrusions at the apex of such blunt tips were demonstrated in bone powder group (Figure 2C, D and Figure 3B, D), while more round-like pore structures were recorded on the smooth surfaces of bone granule group (Figure 2E, F and Figure 3C).

The Sa values of bone fiber, bone powder, and bone granule group were 1.878 μm (1.578–2.415 μm), 5.066 μm (3.891–6.162 μm), and 0.860 μm (0.801–1.452 μm),

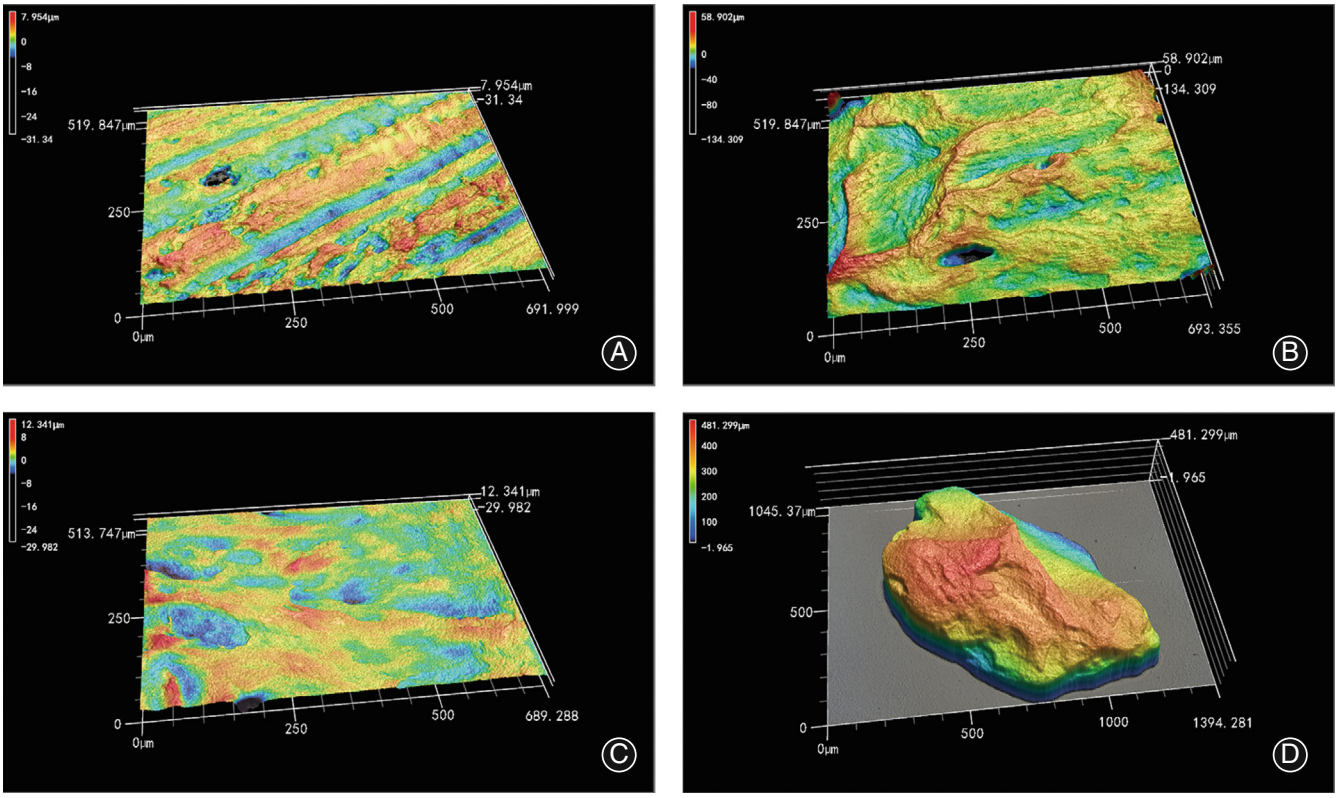

Fig. 3 Micro images of the surface topography of allogenic bone substitutes, including bone fiber (A), bone powder (B and D), bone granule group (C) taken by CLSM

TABLE 1 Mean roughness values of substitute configuration at the regional scale (Midian (IQR 1-IQR3))

Groups	N	Sa† (μm)	*H-value*	*P-value*
Bone fiber	8	1.878 (1.578–2.415)	18.015	**0.000**
Bone powder group	8	5.066 (3.891–6.162)	-	-
Bone granule group	8	0.860 (0.801–1.452)	-	-

* IQR, interquartile range; † Sa, the arithmetic average of the absolute values of the surface height deviations measured from the best fitting plane.

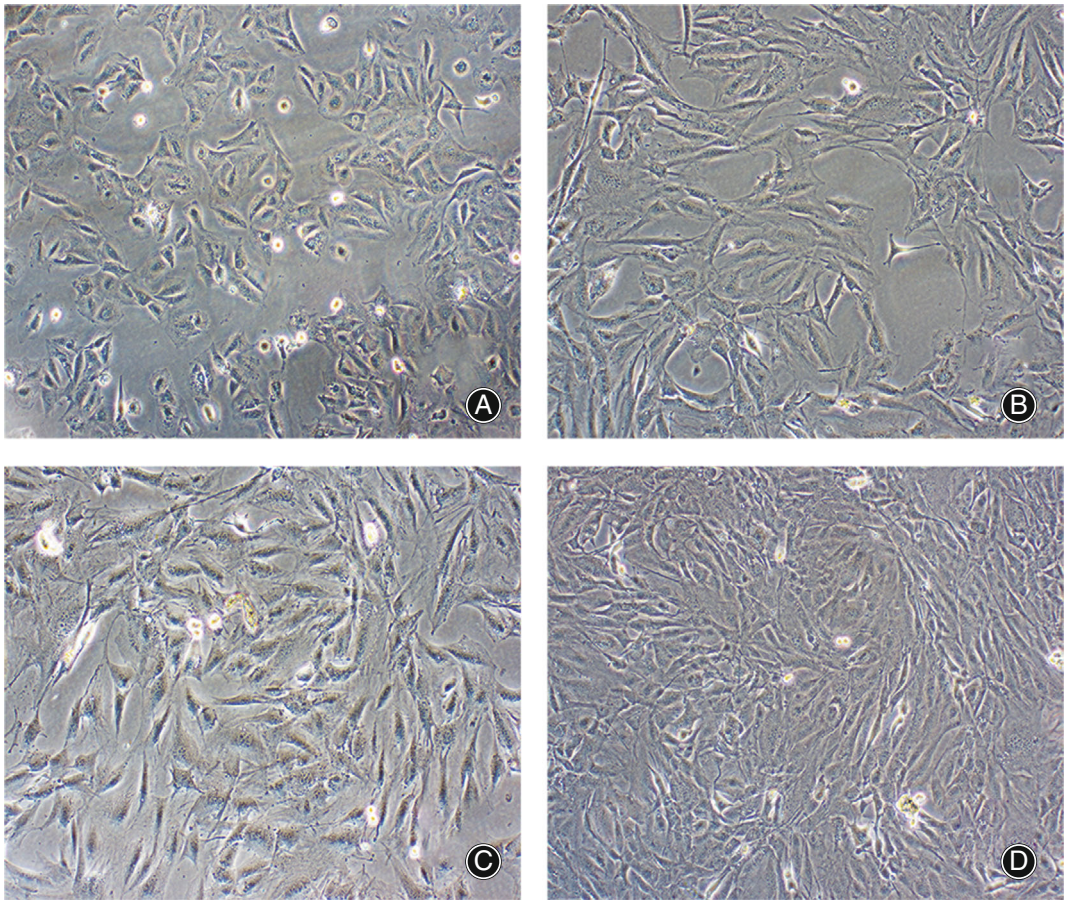

Fig. 4 Representative morphological characteristics, spatial distribution and temporal changes of cells of bone fiber group were captured by inverted phase contrast microscope (magnification = 200 x) at 6 (A), 12 (B), 24 (C) and 48 h (D). Scale bar = 100 μm. (Notably, cells in each group were not exhibited in duplicate due to the fact that the cells were morphologically similar)

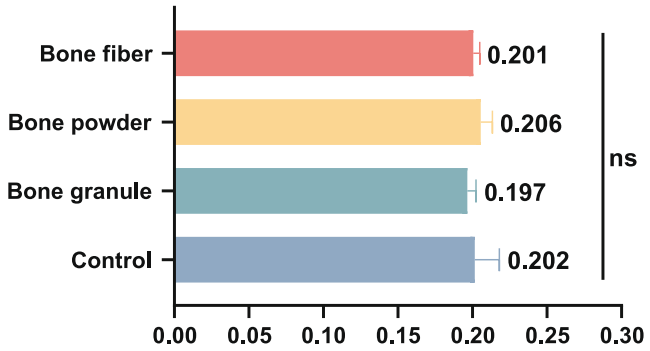

Fig. 5 The optical density (OD) values of osteoblasts during the four groups, including bone fiber, bone powder, bone granule, and control group (untreated cells) for 24 h (n = 5). Data were presented as the mean ± standard deviation. ns: not significant

respectively, in CLSM image results (Table 1). Statistically significant differences were detected between bone powder and bone granule group ($H = 18.015$, $P < 0.001$).

Cell Viability

To access cell viability, the distribution and morphology of the osteoblasts were captured by inverted phase contrast microscope. Morphologically, cells appeared round or oval with a punctiform distribution in bone fiber group at 6 h (Figure 4A), which indicated the cells had not yet spread completely. Cells adhered and proliferated well on the substitutes by 12 h (Figure 4B). Obviously, cells were distributed in sheets or interweaving streams and began to stretch in all directions forming cell aggregates that gradually increased in size. At 24 h (Figure 4C), cells appeared to proliferate slowly and fused with neighboring cell aggregates to form a monolayer covering the substitute surface. By 48 h (Figure 4D), the neatly arranged cells changed morphology from enlarged cells to much smaller and thinner cells. Moreover, no differential changes in morphology were found between cells covering with various bone substitutes, suggesting allogenic bone substitutes have no toxicity towards the cells.

To detect whether allogenic bone substitutes profiles could affect cellular metabolism, CCK-8 assay and the Live/Dead staining kit were performed on bone substitutes. OD

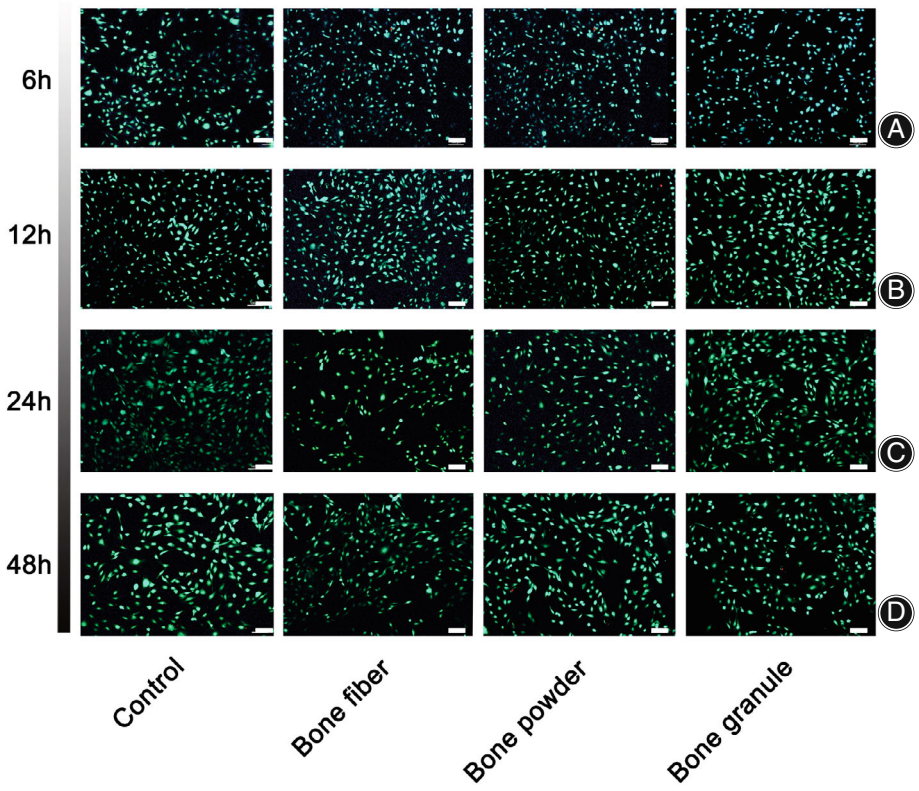

Fig. 6 Biocompatibility evaluation of different substrates including bone fiber, bone powder, bone granule, and control group using the Live/Dead staining kit and confocal fluorescence microscope (magnification = 100 x) at 6 (A), 12 (B), 24 (C) and 48 h (D). Cells stained in green are alive while those stained in red are dead in the merge channels. Scale bar = 100 μm

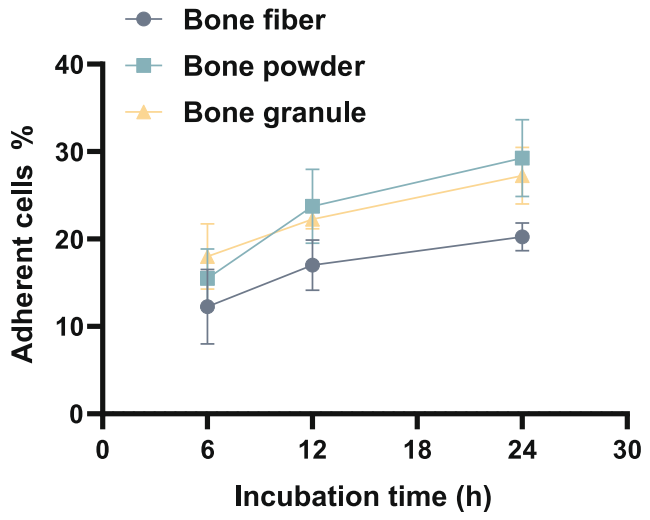

Fig. 7 Initial cell adhesion rate of osteoblasts on various allogenic bone substitutes at different incubation time intervals (6, 12, and 24 h) (n = 5). Data were presented as the mean ± standard deviation. ns: not significant

levels were recorded and analyzed in all groups at 24 h incubation in CCK-8 assay, indicating a good biocompatibility of allogenic bone. And no statistically significant difference was observed in different surfaces of allogenic bone including bone fiber (0.201 ± 0.004), bone powder (0.206 ± 0.008), bone granule (0.197 ± 0.006), and control group (0.202 ± 0.016) ($F = 0.7152$, $P > 0.05$).

Moreover, most of cells were predominantly viable with very few dead cells on the four groups *via* fluorescence imaging for different incubation time (Figure 6), indicating a high biocompatibility of allogenic bone. Results from both cell activity experiments and phase contrast microscopy images indicated a satisfactory cell viability on allogenic bone where fraction configurations had no apparent effect on cell morphology.

Cell Adhesion Analysis

Cell Adhesion Rate

To quantitatively monitor the effect of allogenic bone on the adhesion rate of cells, the average number of cells cultured on the materials were counted and analyzed at 6, 12, and 24h (Figure 7). At 6 h, lower adhesion rate was recorded in bone fiber group (10.3 ± 2.4%) compared to bone powder group (15.8 ± 3.6%) and bone granule group (16.8 ± 1.9%) ($F = 8.155$, $P = 0.008$ and $P = 0.003$, respectively). And at 12h, lower adhesion rate was also shown in bone fiber group (17.0 ± 2.9%) compared to bone powder (23.8 ± 4.2%) and bone granule group (22.3 ± 3.1%) ($F = 5.240$ ‘ $P = 0.001$ and $P = 0.005$, respectively). By 24 h, The rate on bone fiber group (20.3 ± 1.6%) was significantly lower than that of bone powder (29.3 ± 4.4%) and bone granule group (27.3 ± 3.2%) ($F = 10.51$, $P = 0.009$ and $P = 0.034$,

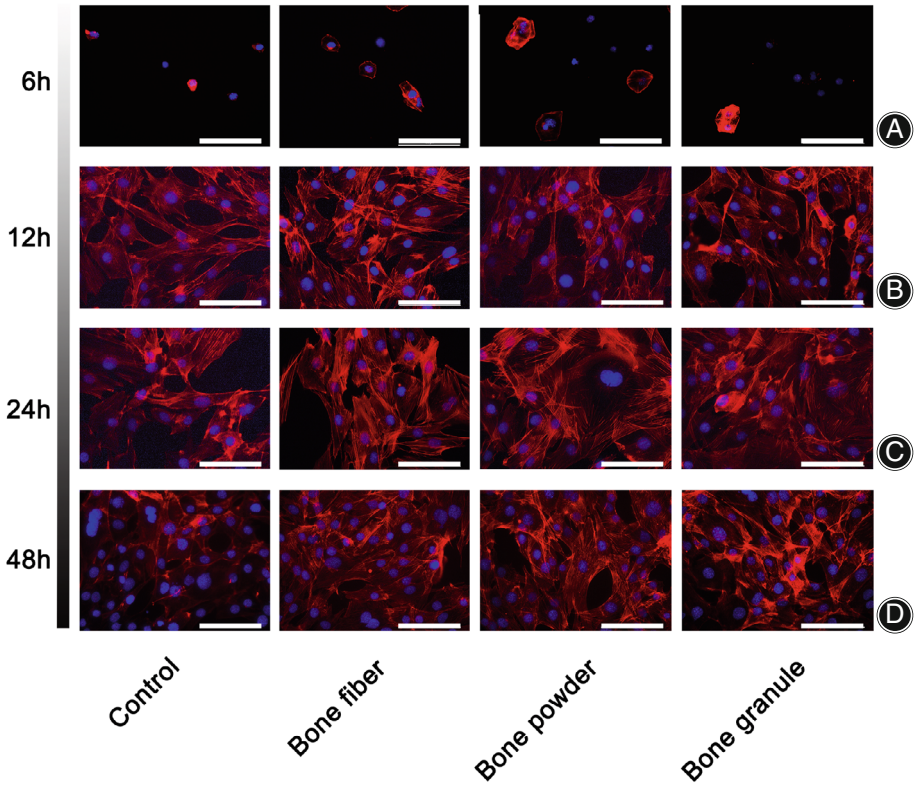

Fig. 8 Location of F-Actin (red) and nuclei (blue) was identified by immunofluorescence staining at 6 h after seeding onto the four groups, and then viewed by inverted fluorescence microscope (magnification = 400 x) at 6 (A), 12 (B), 24 (C), and 48 h (D). Scale bar = 100 μm

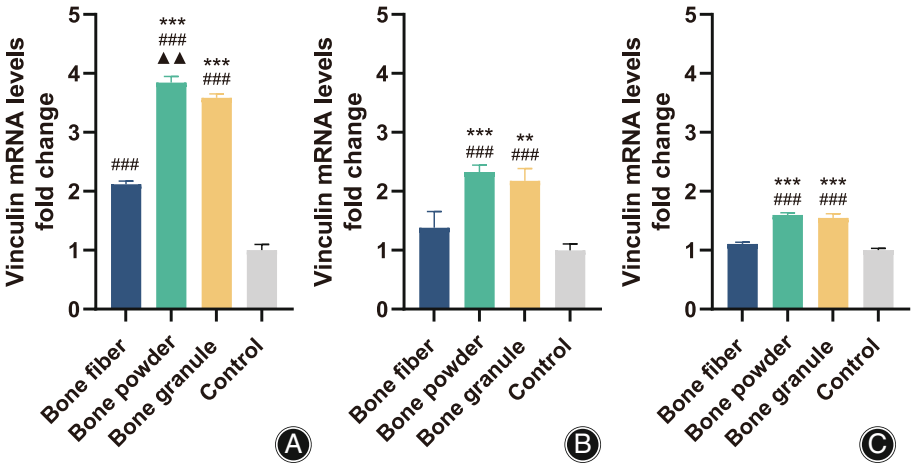

Fig. 9 Expression of vinculin mRNA relative to GAPDH in cells at 6 (A), 12 (B), and 24 h (C) after seeding on various groups. Data analysis was performed using $2^{-\Delta\Delta CT}$ method for relative quantification with GAPDH as the endogenous normalization control (n = 3). GAPDH: glyceraldehyde-3-phosphate dehydrogenase. *P < 0.05, **P < 0.01, ***P < 0.001 compared with bone fiber group; ▲P < 0.05 ▲▲P < 0.01, ▲▲▲P < 0.001 compared with bone granule group, $^{\#}p$ < 0.05, $^{\#\#}p$ < 0.01, $^{\#\#\#}P$ < 0.001 compared with untreated cell group

respectively). However, no significant differences in cell adhesion rate were recorded between bone powder and bone granule group within 24 h incubation.

F-Actin Immunofluorescence Analysis

The cytoskeleton of cells was evaluated by labeling F-actin with rhodamine phalloidin and the nuclei with 4,6-diamidino-2-phenylindole (DAPI), and imaging with a confocal fluorescence microscope. At 6 h, the small number of irregularly shaped cells shown in the field of each group indicated an early stage of the adhesion process (Figure 8A). Allogenic bone substitutes, notably bone powder group, had a polygonal appearance with flaky connection among larger adherent cells, while the control group had oval-shaped cells with reticular connections. The majority of adherent cells reached an extended polygon as clearly stained by phalloidin at 12 h and displayed diffuse cytoskeletons composed of more stretched actin filaments in the proximity of cell membrane (Figure 8B). Multiple large empty spaces were occupied by the spread-out cytoskeleton (Figure 8C and D). Meanwhile, many cells had already intertwined and interconnected to form the reticular appearance.

qPCR Analyses of Vinculin Expression

qPCR was performed to investigate the effect of various substitutes on vinculin protein during the adhesion. The results showed the expression of vinculin mRNA steadily decreased in a time-dependent manner at 6 (Figure 9A), 12 (Figure 9B), and 24 h incubation (Figure 9C). At 6 h, lower vinculin expression of the cells was shown in bone fiber group (2.119 ± 0.052) compared to bone powder (3.842 ± 0.108) and bone granule group (3.585 ± 0.068) ($F = 733.643$, $P < 0.001$ and $P < 0.001$, respectively). Moreover, there was a significant difference in the expression of target gene between bone powder group and bone granule group ($P = 0.006$). By 12 h, bone fiber group (1.381 ± 0.273), as shown in Figure 9B, presented lower vinculin expression compared to bone powder (2.327 ± 0.117) and bone granule group (2.178 ± 0.208) ($F = 34.018$, $P < 0.001$ and $P < 0.001$, respectively). However, there was no significant difference between bone powder and bone granule group ($P > 0.05$). At 24 h, lower vinculin expression was shown in bone fiber group (1.108 ± 0.027) compared to bone powder (1.599 ± 0.035) and bone granule group (1.548 ± 0.070) ($F = 142.344$, $P < 0.001$ and $P < 0.001$, respectively). Three allogenic bone groups, more importantly, presented significantly upregulated genes compared to the control group at three time points (all $P < 0.05$).

Discussions

Main Findings of the Study

The current study provides an overview of the various configurations of three freeze-dried cortical bone, including bone fiber group (0.1 mm × 0.1 mm × 3 mm), bone powder group (0.45–0.9 mm), and bone granule group (3–6 mm), and its potential role regulating the viability, adhesion, and spreading of MC3T3-E1 cells *in vitro* from the phenomenological to the genetic level. Similar OD values of all groups in CCK-8 assay indicated good biocompatibility of these substitutes, among which the bone powder group exhibited a rougher surface than the other groups. In addition, adhesion-related gene (vinculin) was upregulated in three groups compared to the control group. These findings implicated that bone powder and bone granule group might better promote cell adhesion and spreading than bone fiber group.

Characterization and Biocompatibility of Allogenic Bone

Bone graft materials with distinct morphological characteristics are commonly used to regenerate various bone defects over the past decades, but their application is often limited due to the complex defect shape in various clinical conditions. Compared to autologous bone or bone substitute, allogeneic bone substrates have been widely used to repair bone defects for the advantage of abundant sources and easy collection, especially good porosity and osteogenic activity. Few studies, however, focused on osteoblast adhesion *via* estimating the configuration change of allogenic bone substitute, although this property would determine the cell-scaffold interactions and the behavior of major bone cells, which in turn may impact the mineralization and maturation of new bone. Representative macroscopic (Figure 1) and microscopic (Figs 2 and Figure 3) images of different bone substitutes clearly indicated that bone granule group has more round-like pore structures on the smooth surface, and bone fiber has more of the anisotropic wavelike structure than the former and the least pore structures while bone powder group has a greater longitudinal undulation. As MC3T3-E1 cells are commonly used in osteogenesis studies[14,15], they were chosen to incubate with the tested allogenic bone substitutes. The results of CCK-8 assay (Figure 5) and live/dead staining (Figure 6) demonstrated that these allogenic bone substitutes have good cell affinity.

Adhesion Mechanism of Cells on the Material

Cell adhesion, a complex physiological process, greatly affected the cell fate, such as cell proliferation, migration, and differentiation. For most cells, the process of cell adhesion is anchorage-independent, requiring cell-extracellular matrix interactions *via* the formation of actin-associated adhesion complexes and integrin receptors[16]. Accumulating evidence has shown that the adhesion of osteoblastic cell to biomaterials is an indispensable step in the transmission of physicochemical signals from biomaterials into cells, which initiates the osseointegration cascade and regulates the interaction between cells and biomaterials[17].

In fact, tuning the surface properties of biomaterials, especially roughness, can have a profound effect on adhesion and early osseointegration[18]. It is well-documented that the combination of rough surface of the scaffolds with specific ligands on the osteoblast membrane could potentially elicit increased osteoblast adhesion and proliferation[19,20]. The results of roughness (Table 1) demonstrated that bone powder group has larger Sa values (5.03 ± 1.81 μm) compared to bone fiber (2.16 ± 1.03 μm) and bone granule group (1.09 ± 0.23 μm). Besides, the results (Figure 7) revealed that bone powder group had advantages over bone fiber and bone granule group with higher cell adhesion rate *in vitro*. Different results, however, were reported by other studies. It has been reported that when the surface roughness is greater (>2.19 mm), osteoblast adhesion is inhibited because it is difficult to form osteoblastic pseudopodia between the larger crests and grooves[12,21]. Indeed, the surface roughness of the material is an important parameter to consider, whereas pore size and porosity are also essential geometries[22]. Considering bone granule group contained numerous pores captured by SEM (Figure 2E and F), there is sufficient contact area for cell anchoring, which may explain why the adhesion rate of bone granule group is significantly greater than that of bone fiber even though its roughness is the smallest.

Visualization of Cell Adhesion and Unfolding

It has been well-established that osteoblastic cells adhering to biomaterials start in an indirect manner, which is mediated through specific proteins from the extra-cellular matrix, cell membrane, and cytoskeletal proteins, especially F-actin and

vinculin. As the well-organized and complex network structure of protein fibers, the cytoskeleton, especially microfilaments (F-actin), provides a dynamic structural framework and functional elements that are crucial for maintaining normal eukaryotic cell morphology and physiological function (including motility, division, differentiation, and aids in energy conversion, signaling transduction, material transfer, etc.)[11]. Recently, Hung *et al.* have shown that the surface roughness of the material acts as a key element to enhance cell anchoring, and its mechanism may be that rough surface increases hydrophilic properties of the material and thus promotes cell adhesion[23]. Xia *et al.* reported that bone marrow-derived mesenchymal stem cells (BMSCs) were seeded onto two-dimensional nanoporous membranes with controlled nanopore size and roughness to determine the effects of two critical variables on cell behavior, such as adhesion, proliferation, spreading, and differentiation. Fluorescently labeled focal adhesion were applied to clearly visualize the process of cell adhesion. The results showed although both nanopore size and roughness can affect BMSCs, nanopore size yet plays a more significant role than roughness in controlling the behavior of cells[22]. Furthermore, vinculin has binding sites for actin and other proteins such as F-actin, tailin, which can all associate with the actin cytoskeleton[6].

Herein, a typical osteoblastic cell morphology with extended spindle profiles could be observed for cells on different bone substrates, which were very similar to the control group (Figure 8). Moreover, bone powder group increased expression of vinculin, similar to bone granule group, whereas decreased vinculin expression was detected in bone fiber (Figure 9). Interestingly, the expression of vinculin increased and peaked at 6 h, and then decreased across the observed time points. Possibly, some cells over time have started to prepare for proliferation-related gene expression and hinder the expression of genes for adhesion.

Limitations

The current study presents several limitations. First, the subsequent cytological behavior and its mechanism should be further explored, such as migration, proliferation, differentiation, and apoptosis, as the adhesion is only the initiation stage in the complete cytological behavior. Second, the results of this paper have shown that all allogenic bone substitutes favored the adhesion process of cells. However, no *in vivo* experiments, which are indispensable to determine the osteogenesis mechanism of biomaterials, were performed to verify the hypotheis and results of the experiments. Third, the detailed regulatory mechanisms of cell adhesion remain unclear on different modifications of biomaterials, which calls for efforts to define the optimal conditions for osteogenesis and further applications.

Conclusions

Collectively, the effect of different configurations of allogeneic bone substitutes on adhesion process of osteoblasts were dynamically investigated in terms of cell morphology, cell adhesion rate, and the vinculin expression. These data strongly demonstrated that the three allogenic bone substitutes played a facilitating role in the cell adhesion process in which bone powder and bone granule group performed better compared with bone fiber group.

An authorship declaration

All authors listed meet the authorship criteria according to the latest guidelines of the International Committee of Medical Journal Editors, and all authors are in agreement with the manuscript with no competing interests.

Acknowledgements

None.

Funding

None.

References

1. Stevenson S. Biology of bone grafts. Orthop Clin North Am. 1999;30:543–52.
2. Gebhart M, Lane J. A radiographical and biomechanical study of demineralized bone matrix implanted into a bone defect of rat femurs with and without bone marrow. Acta Orthop Belg. 1991;57:130–43.
3. Hua KC, Feng JT, Yang XG, Wang F, Zhang H, Yang L, et al. Assessment of the defatting efficacy of mechanical and chemical treatment for allograft cancellous bone and its effects on biomechanics properties of bone. Orthop Surg. 2020;12:617–30.
4. Lin H, Zhao Y, Sun W, Chen B, Zhang J, Zhao W, et al. The effect of crosslinking heparin to demineralized bone matrix on mechanical strength and specific binding to human bone morphogenetic protein-2. Biomaterials. 2008;29:1189–97.
5. Shi J, Sun J, Zhang W, Liang H, Shi Q, Li X, et al. Demineralized bone matrix scaffolds modified by CBD-SDF-1alpha promote bone regeneration via recruiting endogenous stem cells. ACS Appl Mater Interfaces. 2016;8:27511–22.
6. Chen S, Guo Y, Liu R, Wu S, Fang J, Huang B, et al. Tuning surface properties of bone biomaterials to manipulate osteoblastic cell adhesion and the signaling pathways for the enhancement of early osseointegration. Colloids Surf B Biointerfaces. 2018;164:58–69.
7. Sanz-Herrera JA, Reina-Romo E. Cell-biomaterial mechanical interaction in the framework of tissue engineering: insights, computational modeling and perspectives. Int J Mol Sci. 2011;12:8217–44.
8. Lynch I. Are there generic mechanisms governing interactions between nanoparticles and cells epitope mapping the outer layer of the protein–material interface. Phys A: Stat Mech Appl. 2007;373:511–20.
9. Carisey A, Ballestrem C. Vinculin, an adapter protein in control of cell adhesion signalling. Eur J Cell Biol. 2011;90:157–63.
10. Lin Y, Huang Y, He J, Chen F, He Y, Zhang W. Role of hedgehog-Gli1 signaling in the enhanced proliferation and differentiation of MG63 cells enabled by hierarchical micro−/nanotextured topography. Int J Nanomedicine. 2017;12:3267–80.
11. Dozza B, Lesci IG, Duchi S, Della Bella E, Martini L, Salamanna F, et al. When size matters: differences in demineralized bone matrix particles affect collagen structure, mesenchymal stem cell behavior, and osteogenic potential. J Biomed Mater Res A. 2017;105:1019–33.
12. Anselme K, Bigerelle M, Noel B, Dufresne E, Judas D, Iost A, et al. Qualitative and quantitative study of human osteoblast adhesion on materials with various surface roughnesses. J Biomed Mater Res. 2000;49:155–66.
13. Chen Z, Bachhuka A, Han S, Wei F, Lu S, Visalakshan RM, et al. Tuning chemistry and topography of Nanoengineered surfaces to manipulate immune response for bone regeneration applications. ACS Nano. 2017;11:4494–506.
14. Sun JB, Wang Z, An WJ. Protection of icariin against hydrogen peroxide-induced MC3T3-E1 cell oxidative damage. Orthop Surg. 2021;13:632–40.
15. Sun GJ, Yang SF, Ti YF, Guo GD, Fan GT, Chen FR, et al. Influence of ceramic debris on osteoblast behaviors: An in vivo study. Orthop Surg. 2019;11:770–6.

16. Jones MC, Askari JA, Humphries JD, Humphries MJ. Cell adhesion is regulated by CDK1 during the cell cycle. J Cell Biol. 2018;217:3203–18.
17. Chen Q, Zhang D, Zhang W, Zhang H, Zou J, Chen M, et al. Dual mechanism beta-amino acid polymers promoting cell adhesion. Nat Commun. 2021;12:562.
18. Shen N, Ding H, Bowers R, et al. Surface Micropatterning of Pure Titanium for Biomedical Applications Via High Energy Pulse Laser Peening. J Micro Nanomanuf. 2015;3:011005.
19. Costa DO, Prowse PD, Chrones T, et al. The differential regulation of osteoblast and osteoclast activity by surface topography of hydroxyapatite coatings. Biomaterials. 2013;34:7215–26.
20. Sedlaczek J, Lohmann CH, Lotz EM, Hyzy SL, Boyan BD, Schwartz Z. Effects of low-frequency ultrasound treatment of titanium surface roughness on osteoblast phenotype and maturation. Clin Oral Implants Res. 2017;28: e151–8.
21. Shen N, Ding H, Bowers R, Yu Y, Pence CN, Ozbolat IT, et al. Surface micropatterning of pure titanium for biomedical applications via high energy pulse laser peening. J Micro Nano-Manuf. 2015;3:011005.
22. Xia J, Yuan Y, Wu H, Huang Y, Weitz DA. Decoupling the effects of nanopore size and surface roughness on the attachment, spreading and differentiation of bone marrow-derived stem cells. Biomaterials. 2020;248: 120014.
23. Hung HS, Yu AY, Hsieh SC, et al. Enhanced biocompatibility and differentiation capacity of mesenchymal stem cells on poly(dimethylsiloxane) by topographically patterned dopamine. ACS Appl Mater Interfaces. 2020;12: 44393–406.